ACS APPLIED MATERIALS & INTERFACES

Research Article

www.acsami.org

# Rapid Charge–Discharge Property of $Li_4Ti_5O_{12}$–$TiO_2$ Nanosheet and Nanotube Composites as Anode Material for Power Lithium-Ion Batteries

Ting-Feng Yi,*[,†,‡] Zi-Kui Fang,[†] Ying Xie,*[,‡] Yan-Rong Zhu,[†] and Shuang-Yuan Yang[†]

[†]School of Chemistry and Chemical Engineering, Anhui University of Technology, Maanshan, Anhui 243002, People's Republic of China

[‡]Key Laboratory of Functional Inorganic Material Chemistry, Ministry of Education, School of Chemistry and Materials Science, Heilongjiang University, Harbin 150080, People's Republic of China

Supporting Information

**ABSTRACT:** Well-defined $Li_4Ti_5O_{12}$–$TiO_2$ nanosheet and nanotube composites have been synthesized by a solvothermal process. The combination of in situ generated rutile–$TiO_2$ in $Li_4Ti_5O_{12}$ nanosheets or nanotubes is favorable for reducing the electrode polarization, and $Li_4Ti_5O_{12}$–$TiO_2$ nanocomposites show faster lithium insertion/extraction kinetics than that of pristine $Li_4Ti_5O_{12}$ during cycling. $Li_4Ti_5O_{12}$–$TiO_2$ electrodes also display lower charge-transfer resistance and higher lithium diffusion coefficients than pristine $Li_4Ti_5O_{12}$. Therefore, $Li_4Ti_5O_{12}$–$TiO_2$ electrodes display lower charge-transfer resistance and higher lithium diffusion coefficients. This reveals that the in situ $TiO_2$ modification improves the electronic conductivity and electrochemical activity of the electrode in the local environment, resulting in its relatively higher capacity at high charge–discharge rate. $Li_4Ti_5O_{12}$–$TiO_2$ nanocomposite with a Li/Ti ratio of 3.8:5 exhibits the lowest charge-transfer resistance and the highest lithium diffusion coefficient among all samples, and it shows a much improved rate capability and specific capacity in comparison with pristine $Li_4Ti_5O_{12}$ when charging and discharging at a 10 C rate. The improved high-rate capability, cycling stability, and fast charge–discharge performance of $Li_4Ti_5O_{12}$–$TiO_2$ nanocomposites can be ascribed to the improvement of electrochemical reversibility, lithium ion diffusion, and conductivity by in situ $TiO_2$ modification.

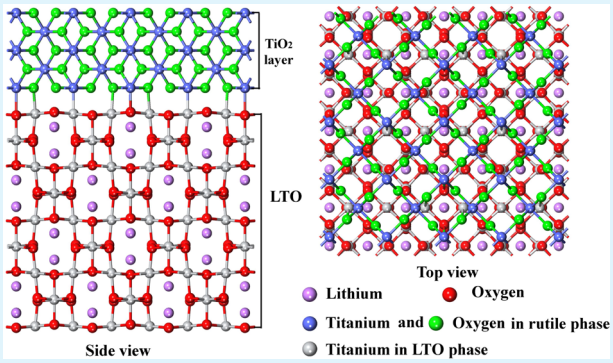


**KEYWORDS:** *lithium-ion battery, $Li_4Ti_5O_{12}$, $TiO_2$, rapid charge–discharge property, rate capability*

## 1. INTRODUCTION

Over the past 20 years, lithium-ion batteries (LIBs) have been well-developed for portable electronic devices as one of the reliable green energy sources because of their high energy density and relatively simple reaction mechanism. Today, it is necessary to further promote the development of LIB materials from the aspects of energy density, cycling performance, and safety issues in order to widely enable the application of lithium-ion batteries in large-scale high-power system such as the plug-in electric vehicle (PEV), plug-in hybrid electric vehicle (PHEV), or hybrid electric vehicle (HEV).[1−3] Carbonaceous material, used widely in portable electronic devices, is the most common anode material for LIBs due to its desirable charge potential profile, good cyclability, and abundant reserves in the natural world.[4,5] However, there are still some safety concerns because Li dendrites are likely to be formed on carbon material surface after long charge–discharge operations. Recently, spinel lithium titanium oxide ($Li_4Ti_5O_{12}$, LTO) has attracted much interest owning to the potential application as an anode material for power lithium-ion batteries.[6−8] $Li_4Ti_5O_{12}$ shows a stable and high working potential (about 1.55 V vs Li/$Li^+$), and then the formation of the solid-electrolyte interphase (SEI) layer (usually occurring below 1.0 V Li/$Li^+$) and the deposition of lithium dendrites can be effectively suppressed.[9,10] In addition, $Li_4Ti_5O_{12}$ also exhibits excellent safety, high structural stability, and thermodynamic stability due to its zero volume change in the charge–discharge process.[11,12] However, the inherently kinetic problems, that is, low electrical conductivity and lithium diffusion coefficient, limit its rate capability.[13,14] Hence, many efforts have been devoted to modify LTO using an alien ion (such as $Na^+$,[15] $Zn^{2+}$,[16] $Ca^{2+}$,[17] $Mg^{2+}$,[18] $Ni^{2+}$,[19] $Al^{3+}$,[20] $Sc^{3+}$,[21] $La^{3+}$,[22] $Ru^{4+}$,[23] $Zr^{4+}$,[24] $V^{5+}$,[25] $Nb^{5+}$,[26] $W^{6+}$,[27] $Mo^{6+}$,[28] and $F^-$[29]) in Li, Ti, or O sites, or by introducing a second phase (such as carbon,[30] graphene,[31] Cu,[32] Ag,[33] Au,[34] $TiO_2$,[10,35,36] $ZrO_2$,[37] TiN,[38] $AlF_3$,[39] $Li_{3x}La_{(2/3)-x}TiO_3$,[40] and PEDOT[41]), or by synthesizing nano-

Received: August 26, 2014
Accepted: October 20, 2014
Published: October 20, 2014

  

sized materials.[42,43] Rutile titanium oxide ($TiO_2$) has been considered as one alternative anode material for safe lithium-ion batteries with a high theoretical capacity of 335 mAh $g^{-1}$ corresponding to one lithium insertion into the lattice of $TiO_2$ per formula,[44]

$$TiO_2 + Li^+ + e^- \Leftrightarrow LiTiO_2 \quad (1)$$

Rutile $TiO_2$ exhibits a fast Li insertion/extraction kinetic along the *c* axis channels during charge−discharge cycling. The theoretical $Li^+$ diffusion coefficient along the *c* axis is reported to be $10^{-6}$ $cm^2$ $s^{-1}$, which is much higher than that of $Li_4Ti_5O_{12}$.[44−46] In the previous reports, spinel $Li_4Ti_5O_{12}$ has been synthesized by solid-state method,[15,16] sol−gel method,[47] solution-combustion synthesis,[48] molten-salt synthesis method,[49] rheological phase reaction[50] and hydrothermal synthesis.[51] The synthesis of $Li_4Ti_5O_{12}$ mentioned above requires a high temperature (over 800 °C), and the product usually exhibits a micron or submicron size. Unfortunately, the cycling life and power density of $Li_4Ti_5O_{12}$ with a micron or submicron size are relatively low because a large polarization is expected during rapid charge−discharge processes. This polarization is mainly derived from a slow lithium diffusion in the active material and a large resistance of the electrolyte when the charging−discharging rate is increased.[52] As we know, nanostructured electrode materials can provide high surface areas and short diffusion paths for ionic transport and electronic conduction.[53] Hence, it is important to focus on the size and shape control of the nanostructured electrode materials by developing effective synthetic techniques. Compared with the methods mentioned above, $Li_4Ti_5O_{12}$ synthesized by solvothermal processes can be obtained at about 500−600 °C. The solvothermal processes usually have many advantages such as short processing times, fast reaction kinetics, high crystallinity and phase purity, homogeneous and narrow particle-size distributions, and low postcalcination temperature. Hence, it can be concluded that solvothermal processes are environmentally benign, cost-effective, and easily scalable.[54] Until now, to our best knowledge, no dual-phase $Li_4Ti_5O_{12}$−rutile $TiO_2$ nanosheets or nanotubes have been reported in lithium-ion battery application. Herein, facile solvothermal syntheses of $Li_4Ti_5O_{12}$ and dual-phase $Li_4Ti_5O_{12}$−rutile and anatase $TiO_2$ nanosheets and nanotubes as anode materials, were proposed. The as-prepared $Li_4Ti_5O_{12}$ and dual phase $Li_4Ti_5O_{12}$−rutile and anatase $TiO_2$ anode materials present high reversible capacity and good cycling performance during the rapid charge−discharge process, indicating a promising application as anode materials for power lithium-ion batteries.

## 2. EXPERIMENTAL SECTION

**2.1. Material Preparation.** $Li_4Ti_5O_{12}$ and dual phase $Li_4Ti_5O_{12}$−rutile and anatase $TiO_2$ nanosheets and nanotubes were prepared by in situ solvothermal processes. The overall fabrication procedures of nanosheets and nanotubes are schematically illustrated in Figure 1.

Analytical-grade $Ti(OC_3H_7)_4$ (AR, ≥99%) and $LiOH·H_2O$ (AR, 98%) were used as raw materials. First, 10 mmol $Ti(OC_3H_7)_4$ and a certain amount of $LiOH·H_2O$ were added to 25 mL of polyethylene glycol (PEG 400) at room temperature. The molar ratios of Li/Ti are 3.8:5, 4:5, and 4.5:5, respectively. According to the molar ratios of Li/Ti, the samples denote as LTO-TO1, LTO-TO2, and LTO, respectively. The mixed solution was vigorously stirred about 12 h to make LiOH dissolved in PEG 400 in a closed container. Then, 50 mL of deionized water was added to the container, and the mixture was strongly stirred for about 2 min. The resulting suspension was transferred to a Teflon-lined stainless steel autoclave and heated at 180 °C for 40 h. The powder deposited at the bottom of the reactor was collected by centrifugation, and washed with ethanol three to four times. After the powders dried in vacuum at 80 °C for 5−6 h, they were annealed at 550 °C for 6 h in air to form final products.

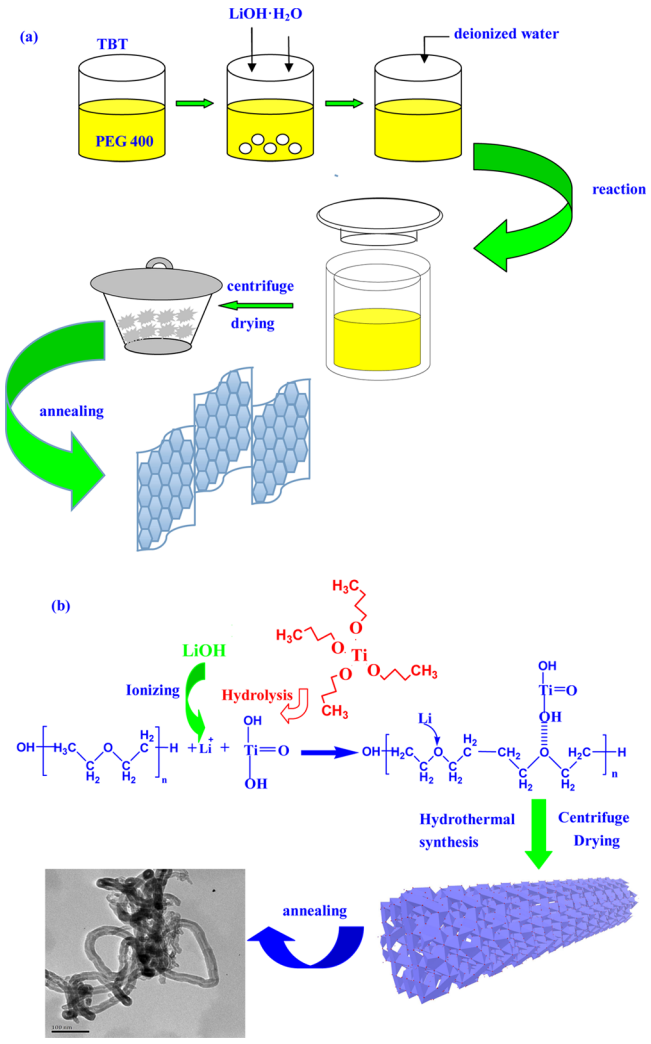


**Figure 1.** Fabrication procedures of $Li_4Ti_5O_{12}$ and dual phase $Li_4Ti_5O_{12}$−rutile $TiO_2$ (a) nanosheets and (b) nanotubes in this study.

**2.2. Battery Preparation.** A CR2025 coin-cell assembly was used for the electrochemical characterization. A slurry was formed by mixing the active material (80%), super P conductive carbon (10%), and binder (10 wt % polyvinylidene fluoride, dissolved in *N*-methyl-2-pyrrolidone). After being coated onto the Cu foil, the film was dried in a vacuum oven at 110 °C for 10 h and then cut into discs with a radius of 7 mm. The loading weight was about 2 mg $cm^{-2}$, and the thickness of electrode prepared in this study is about 30 $\mu$m. The half-cells were assembled with a composite cathode and a metallic lithium anode separated by porous polypropylene film (Celgard 2300) filled with 1 M $LiPF_6$ in ethylene carbonate/dimethyl carbonate (1:1 v/v) solution.

**2.3. Material Characterization and Electrochemical Tests.** X-ray diffractometry (XRD) measurements were performed on a Rigaku instrument with Cu K$\alpha$ radiation. Particle sizes, morphologies, and microstructures were examined using a scanning electron microscope (FESEM, Hitachi-4300) and a transmission electron microscope (TEM, JEOL-2010F). Cyclic voltammetry (CV) test of all half cells charge−discharged at 10 C rate after 200 cycles was carried out on a Princeton P4000 electrochemical workstation with a voltage between 1.0 and 2.5 V under a scanning rate of 0.2 mV $s^{-1}$. Electrochemical impedance spectroscopy (EIS) is measured by a Princeton P4000 electrochemical working station over a frequency range from 0.1 Hz to 10 kHz at a potentiostatic signal amplitude of 5 mV. The charge−

discharge measurements were recorded on multichannel Land Battery Test System (Wuhan Jinnuo, China) at room temperature in a 1.0−2.5 V (vs $Li/Li^+$) range at different charge−discharge rates (where 1 C = 175 mA $g^{-1}$).

## 3. RESULTS AND DISCUSSION

XRD patterns of the pristine $Li_4Ti_5O_{12}$ and dual phase $Li_4Ti_5O_{12}$−rutile and anatase $TiO_2$ composites are shown in Figure 2. The XRD patterns of all samples are in good agreement with the spinel $Li_4Ti_5O_{12}$, with all of the diffraction peaks indexed to the cubic spinel of $Fd\bar{3}m$ space group.

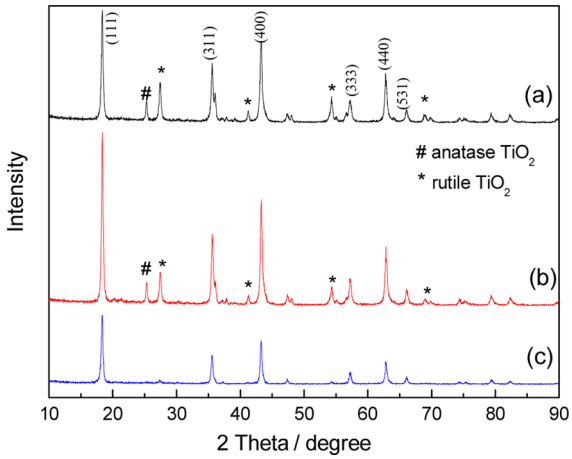


**Figure 2.** XRD patterns of the as-prepared samples with different molar ratio between Li and Ti: (a) Li/Ti = 3.8:5, (b) Li/Ti = 4:5, and (c) Li/Ti = 4.5:5.

From Figure 2, the diffraction peaks at 27.5°, 41.3°, 54.4°, and 69.0° can be ascribed to the rutile $TiO_2$ (JCPDS No. 21−1276), and the small diffraction peak at 27.5° can be ascribed to the anatase $TiO_2$ (JCPDS No. 21-1272). With an increasing molar ratio of Ti in the solution, the XRD peaks of rutile $TiO_2$ became stronger, manifesting that the amount of rutile $TiO_2$ becomes larger. As we know, water has much higher polarity than PEG. The large amount of PEG in the solvent can hinder the reaction between the solvated $Li^+$ ions and hydrolyzed titanium hydroxide precursor, resulting in a formation of dual phase $Li_4Ti_5O_{12}$−rutile $TiO_2$ composites. Hence, the excess solvated $Li^+$ ions in the mixed solution of water and PEG can react with titanium hydroxide and then generate the Li-rich product ($Li_4Ti_5O_{12}$). From Figure 2c, it can be seen that pure $Li_4Ti_5O_{12}$ can be generated when the molar ratio of Li to Ti is 4.5:5 (excess 10%).

Figure 3 shows the general morphologies of as-prepared $Li_4Ti_5O_{12}$ and $Li_4Ti_5O_{12}$−rutile $TiO_2$ composites. It is apparent that the morphologies of three samples are similar, and all samples show the aggregate nanoparticle with uniform particle distribution. The detailed microstructures of all of the as-prepared samples are shown in the TEM images in the insets of Figure 3.

It can be seen that all nanocomposites consist of irregular nanosheets and nanotubes. The nanosheets and nanotubes are tightly attached to each other, thus constructing a typical conductive network. Interestingly, the molar ratio between Li and Ti also influences the morphology of the products. It is obvious that the sample $Li_4Ti_5O_{12}$−$TiO_2$ (Li/Ti = 3.8:5) has more nanotubes than other samples. As a general rule, a one-dimensional nanotube has more surfaces than a two-dimensional nanosheet. Hence, the sample $Li_4Ti_5O_{12}$−$TiO_2$ (Li/Ti = 3.8:5) may have a larger specific surface area than other samples. The large specific surface area can supply sufficient active sites to boost the electrochemical reactions and the transportations of the solvated $Li^+$ ions in the pores, which will be benefit for the rate performance of $Li_4Ti_5O_{12}$.[55]

Figure 4 shows the initial galvanostatic charge and discharge curves of dual-phase $Li_4Ti_5O_{12}$−$TiO_2$ and single-phase $Li_4Ti_5O_{12}$ at a rate of 0.5 C between 1.0 and 2.5 V (vs $Li/Li^+$).

The flat plateau position of the charge and discharge curves for all samples at about 1.7 and 1.5 V can be attributed to the redox reactions of $Ti^{4+}/Ti^{3+}$ in $Li_4Ti_5O_{12}$. In addition, it can be noted that a small charge plateau corresponding to the cathodic potentials of rutile $TiO_2$ is observed at about 2.1 V for the $Li_4Ti_5O_{12}$−$TiO_2$ electrodes.[56,57] These peaks can be ascribed to the phase transformation from $TiO_2$ to $LiTiO_2$, as shown in Figure 5a.

It can be found that the first discharge capacities of the $Li_4Ti_5O_{12}$−$TiO_2$ electrodes are 20−25 mAh $g^{-1}$ higher than that of $Li_4Ti_5O_{12}$ (Li/Ti = 4.5:5). It is obvious that the discharge capacities of the $Li_4Ti_5O_{12}$−$TiO_2$ electrodes exceed the theoretical capacity (175 mAh $g^{-1}$). The extra capacity may be due to the lithium ion insertion into and extraction from $TiO_2$.

Figure 6 shows the $dQ/dV$ versus voltage plots of the as-prepared samples derived from Figure 5 with different Li and Ti molar ratios between 1.0 and 2.5 V.

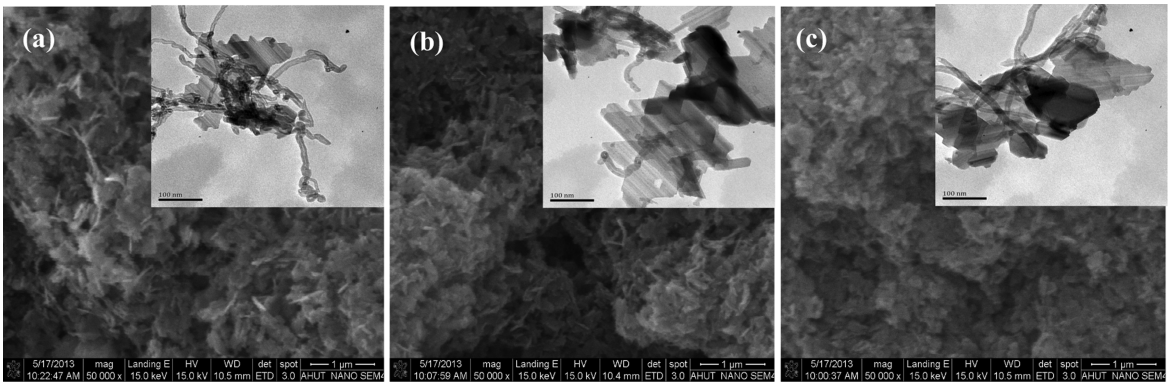


**Figure 3.** SEM and TEM images of the as-prepared samples with different molar ratio between Li and Ti: (a) Li/Ti = 3.8:5, (b) Li/Ti = 4:5, and (c) Li/Ti = 4.5:5.

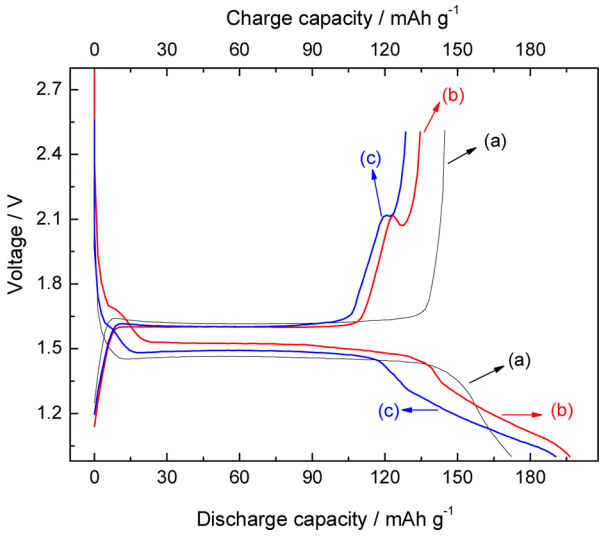


**Figure 4.** Initial galvanostatic charge and discharge curves of dual-phase $Li_4Ti_5O_{12}$–$TiO_2$ and single-phase $Li_4Ti_5O_{12}$ at a rate of 0.5 C; (a) Li/Ti = 4.5:5, (b) Li/Ti = 4:5, and (c) Li/Ti = 3.8:5.

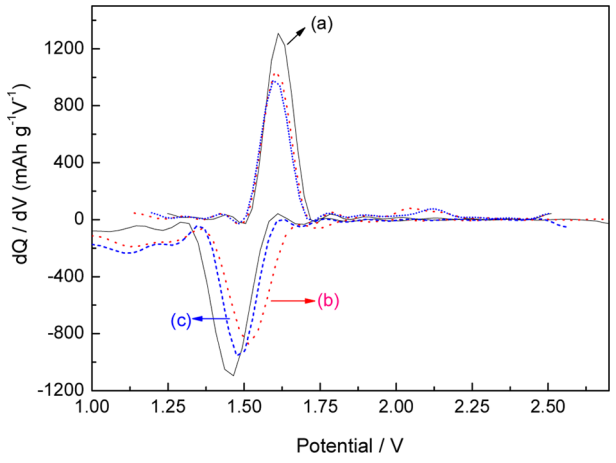


**Figure 6.** Differential capacity vs voltage plots of the as-prepared samples with different molar ratio between Li and Ti: (a) Li/Ti = 4.5:5, (b) Li/Ti = 4:5, and (c) Li/Ti = 3.8:5.

From Figure 6, it is observed that the electrochemical insertion of lithium into $Li_4Ti_5O_{12}$ is a two-phase process that forms a solid solution between $Li_4Ti_5O_{12}$ and $Li_7Ti_5O_{12}$. Figure 5b shows the phase transformation between $Li_4Ti_5O_{12}$ and $Li_7Ti_5O_{12}$. According to Figure 5b, the 32e positions are taken by O atoms, five-sixths of the 16d positions are taken by Ti, and the rest of the 16d positions are taken by Li atoms. The 8a sites are occupied by Li, while the 16c sites are empty, and the structure can be denoted as $[Li_3]_{8a}[\ ]_{16c}[Ti_5Li]_{16d}[O_{12}]_{32e}$ ($Li_4Ti_5O_{12}$). After lithium insertion, a new phase $Li_7Ti_5O_{12}$ can be formed. It can be denoted as $[\ ]_{8a}[Li_6]_{16c}[Ti_5Li]_{16d}[O_{12}]_{32e}$ ($Li_7Ti_5O_{12}$), corresponding to the 1.5 V plateau, and the electrochemical energy comes from reversible redox reactions between $Ti^{3+}$ and $Ti^{4+}$. Figure 6 shows that the potential differences of peaks for $Li_4Ti_5O_{12}$–$TiO_2$ electrodes are less than that of single-phase $Li_4Ti_5O_{12}$, indicating that the former has less polarization associated with $Li^+$ insertion/extraction than the latter. This observation suggests that the $Li_4Ti_5O_{12}$–$TiO_2$ electrodes are beneficial from the reversible intercalation and deintercalation of $Li^+$, leading to the improvement of the reversibility.

Figure 7 shows the cycling performance of the $Li_4Ti_5O_{12}$–$TiO_2$ nanocomposites and $Li_4Ti_5O_{12}$ at different charge–discharge rates. The charge rate is the same as the discharge rate. As shown in Figure 7, all samples exhibit high rate performances. $Li_4Ti_5O_{12}$ sample exhibits much higher rate capability than $Li_4Ti_5O_{12}$–$TiO_2$ electrodes below 5 C charge–discharge rates. For instance, $Li_4Ti_5O_{12}$–$TiO_2$ with Li/Ti = 4:5 and Li/Ti = 3.8:5 offer a capacity of about 103 and 109 mAh $g^{-1}$, respectively, while pristine $Li_4Ti_5O_{12}$ delivers a remarkable capacity of 130 mAh $g^{-1}$ at 3 C charge–discharge rate after 120 cycles. With a further increase of charge–discharge rate to 5 C, the discharge capacity of $Li_4Ti_5O_{12}$ still reaches 125 mAh $g^{-1}$,

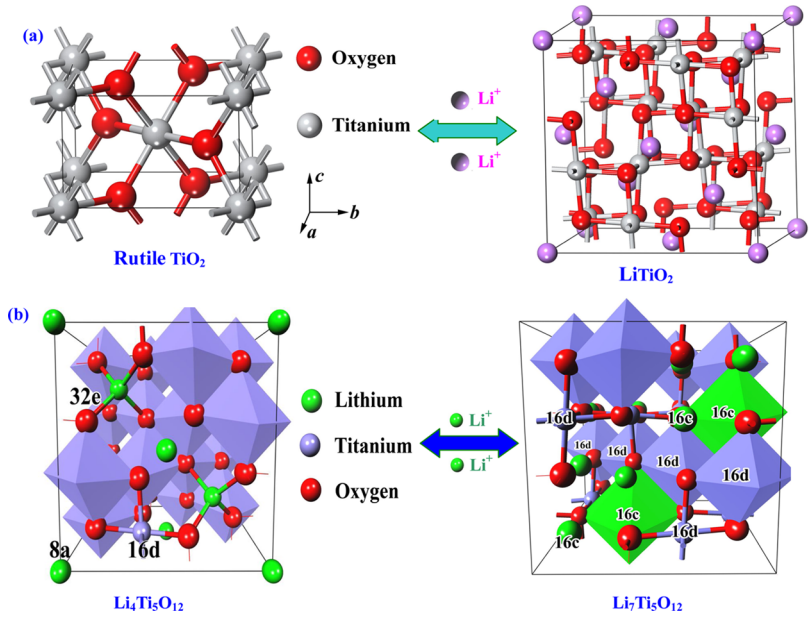


**Figure 5.** Structure transformation of (a) rutile $TiO_2$ and $LiTiO_2$ and (b) $Li_4Ti_5O_{12}$ and $Li_7Ti_5O_{12}$ during charge and discharge. In $Li_4Ti_5O_{12}$ system, O and Li occupy 32(e) and 8(a) sites, respectively; 16(d) sites are occupied by Ti and Li with a ratio of 5:1.


dx.doi.org/10.1021/am5057568 | ACS Appl. Mater. Interfaces 2014, 6, 20205–20213

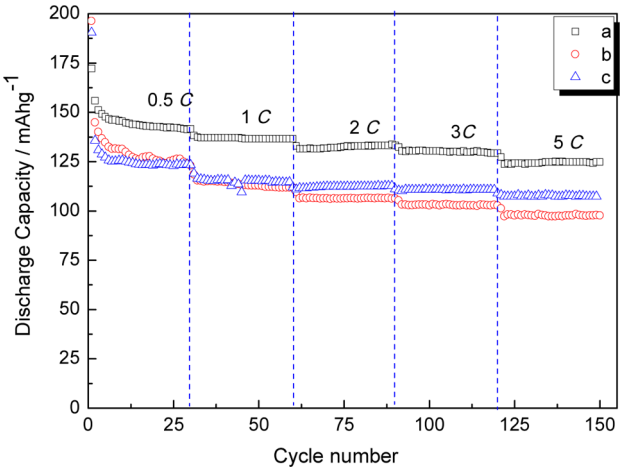


**Figure 7.** Cycling performances of the as-prepared samples with different molar ratio between Li and Ti at different charge–discharge rates in the potential range from 1.0 to 2.5 V; (a) Li/Ti = 4.5:5, (b) Li/Ti = 4:5, and (c) Li/Ti = 3.8:5.

even after 150 cycles. The discharge capacities of $Li_4Ti_5O_{12}$–$TiO_2$ nanocomposites and $Li_4Ti_5O_{12}$ at 3 C charge–discharge rate are even higher than the reported capacities at 2 C charge–discharge rate.[58]

These may be explained by the facts that (1) nanoprimary particles of $Li_4Ti_5O_{12}$–$TiO_2$ nanocomposites and $Li_4Ti_5O_{12}$ allow fast lithium diffusions because of the short lithium transport pathway within the nanoparticle, and in turn, the cycling stability was enhanced because of fewer structural distortions at the electrode surface; (2) nano particles can enhance interfacial reactivity and provide more interfacial area for contact within the liquid electrolyte and can increase the opportunity for lithium ions to intercalate back the host structure; and (3) well-dispersed $Li_4Ti_5O_{12}$–$TiO_2$ and $Li_4Ti_5O_{12}$ nanotubes are adequate in building long-range conducting scaffolds because of their unique 1D tubular morphology, which results in high-capacity retention.

As we know, high rate performance is important for applications in which fast charge and discharge are needed, such as in HEV and PHEV applications.[59] Hence, it is important to focus on the fast charge–discharge property of $Li_4Ti_5O_{12}$–$TiO_2$ nanocomposites. Figure 8 gives more information about the fast charge–discharge performances of the $Li_4Ti_5O_{12}$–$TiO_2$ nanocomposites and $Li_4Ti_5O_{12}$, carried out at 10 C charge–discharge rate.

Compared with those shown in Figure 8, the discharge capacities of $Li_4Ti_5O_{12}$ decrease quickly with increasing discharge rate due to the large polarization of electrodes at high rate, whereas $Li_4Ti_5O_{12}$–$TiO_2$ nanocomposites decrease slowly at the same rate. The discharge capacities of $Li_4Ti_5O_{12}$–$TiO_2$ nanocomposites with Li/Ti = 4:5 and Li/Ti = 3.8:5 are 79 and 96 mAh $g^{-1}$, respectively, after 200 cycles. It can still retain 100% of the initial capacity, exhibiting an excellent cycle stability at high charge–discharge rate. It is interesting that the discharge capacity increases with increasing content of $TiO_2$. On the contrary, the discharge capacity of pristine $Li_4Ti_5O_{12}$ is only 71 mAh $g^{-1}$ after 200 cycles, revealing a poor rate-capability at a high charge–discharge rate. It is reasonable to assume that the high rate capacity of the $Li_4Ti_5O_{12}$–$TiO_2$ nanocomposites is related to the modification of $TiO_2$.

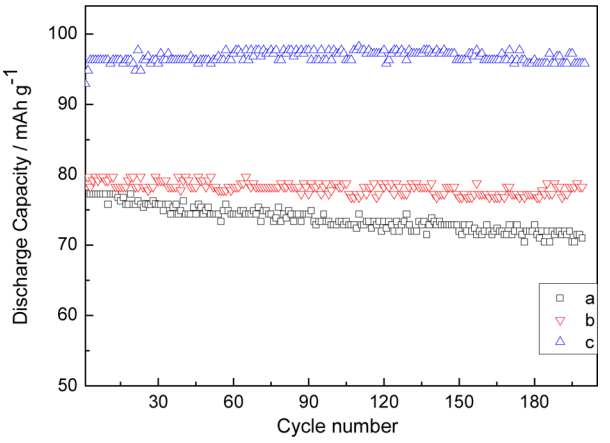


**Figure 8.** Cycling performances of the as-prepared samples with different molar ratio between Li and Ti at 10 C charge–discharge rates in the potential range from 1.0 to 2.5 V; (a) Li/Ti = 4.5:5, (b) Li/Ti = 4:5, and (c) Li/Ti = 3.8:5.

Figure 9 presents the cyclic voltammetry (CV) of the composite anodes charge–discharged at 10 C rate after 200 cycles.

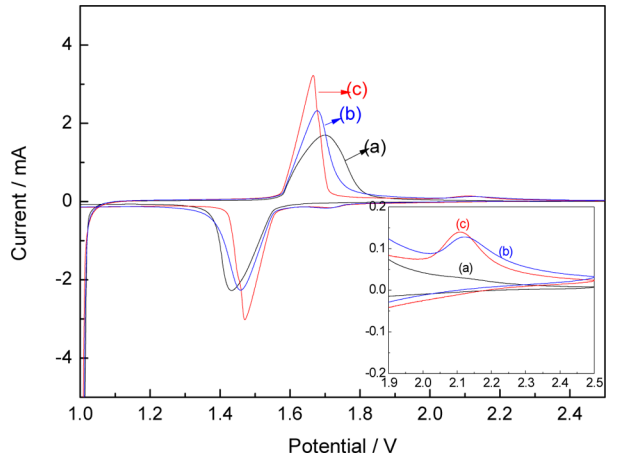


**Figure 9.** Cyclic voltammetry (CV) of the composite anodes with different molar ratio between Li and Ti at 10 C charge–discharge rates after 200 cycles; (a) Li/Ti = 4.5:5, (b) Li/Ti = 4:5, and (c) Li/Ti = 3.8:5.

The oxidation and reduction peaks of $Li_4Ti_5O_{12}$–$TiO_2$ nanocomposites are similar to those of pristine $Li_4Ti_5O_{12}$. The redox current peaks at about 1.5 V/1.6 V correspond to the two-phase reaction between spinel structure of $Li_4Ti_5O_{12}$ and rock-salt structure of $Li_7Ti_5O_{12}$. As shown in Figure 9 b,c, the oxidation peaks of $Li_4Ti_5O_{12}$–$TiO_2$ nanocomposites at 2.09 V correspond to the cathodic peak potential of $TiO_2$,[60,61] which is consistent with the results of charge profile (Figure 4b,c).

The potential difference between the anodic and cathodic peaks can reflect the polarization degree of the electrode.[62] It can bee seen that $Li_4Ti_5O_{12}$–$TiO_2$ nanocomposites show high and sharp cathodic and anodic peaks after even 200 cycles, indicating good electrode kinetics. $Li_4Ti_5O_{12}$–$TiO_2$ nanocomposites show much smaller potential difference than pristine $Li_4Ti_5O_{12}$. This reveals that $TiO_2$ modification can reduce the electrode polarization. $Li_4Ti_5O_{12}$–$TiO_2$ nanocomposite (Li/Ti = 3.8:5) shows the smallest potential difference after 200 cycles among all samples. This implies


dx.doi.org/10.1021/am5057568 | ACS Appl. Mater. Interfaces 2014, 6, 20205–20213

that it shows the smallest electrode polarization during high rate charge−discharge among all samples. This may be the reason that the $Li_4Ti_5O_{12}$−$TiO_2$ nanocomposite (Li/Ti = 3.8:5) shows the highest rate capacity and cycling stability during fast charge−discharge among all samples (Figure 8).

EIS spectra used to evaluate electrode impedance of the composite anodes are shown in Figure 10. The high-frequency

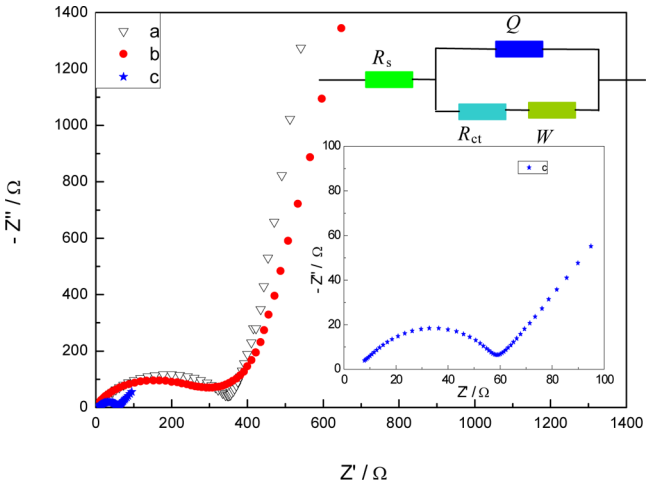


**Figure 10.** Electrochemical impedance spectra of the as-prepared samples with different molar ratio between Li and Ti: (a) Li/Ti = 4.5:5, (b) Li/Ti = 4:5, and (c) Li/Ti = 3.8:5. (Insets) Equivalent circuit and enlarged Niquist plot of $Li_4Ti_5O_{12}$−$TiO_2$ nanocomposites with Li/Ti = 3.8:5.

intercept at the real axis corresponding to the ohmic resistance of the cell is caused by the electrolyte ($R_s$), while the capacitive loop is mainly contributed from the charge transfer resistance ($R_{ct}$). The linear Warburg region in the low-frequency region was associated with $Li^+$ diffusion within the bulk of $Li_4Ti_5O_{12}$.[63−65] The fitted result is shown in Table 1. The $R_s$

**Table 1. Fitted Result from EIS**

| | $Li_4Ti_5O_{12}$ | $Li_4Ti_5O_{12}$−$TiO_2$(Li/Ti = 4:5) | $Li_4Ti_5O_{12}$−$TiO_2$(Li/Ti = 3.8:5) |
|---|---|---|---|
| $R_s$ /Ω | 19.1 | 2.8 | 6.6 |
| $R_{ct}$/Ω | 244 | 245 | 49 |
| $D_{Li}$/cm$^2$ s$^{-1}$ | $7.7 \times 10^{-16}$ | $1.0 \times 10^{-15}$ | $6.8 \times 10^{-14}$ |

reflects electric conductivity of the electrolyte, separator, and electrodes. $Li_4Ti_5O_{12}$−$TiO_2$ electrodes show lower ohmic resistance than that of pristine $Li_4Ti_5O_{12}$, indicating that $TiO_2$ modification reduces the resistance between the electrode and electrolyte. In addition, $Li_4Ti_5O_{12}$−$TiO_2$ composite (Li/Ti = 3.8:5) exhibits the lowest charge transfer resistance among all samples, as shown in Table 1.

To further show the effects of $TiO_2$ modification on the kinetics of the electrode processes, we present EIS result of $Li_4Ti_5O_{12}$ and $Li_4Ti_5O_{12}$−$TiO_2$ (Li/Ti = 3.8:5) samples charge−discharged at 10 C rate after 100 cycles at 100% charge state (charged to 2.5 V) in Figure S1 (Supporting Information). $Li_4Ti_5O_{12}$−$TiO_2$ composite (Li/Ti = 3.8:5) also exhibits lower charge transfer resistance than pristine $Li_4Ti_5O_{12}$(Li/Ti = 4.5:5). This reveals that the $TiO_2$ modification improves the electronic conductivity of the electrode in the local environment. This indicates that the electrochemical activity is greatly increased, resulting in a relatively higher capacity at a high charge−discharge rate.

The lithium ion diffusion coefficient ($D_{Li}$) can be calculated according to the following equation:[63]

$$D_{Li} = \frac{R^2T^2}{2A^2n^4F^4C_{Li}^2\sigma^2} \quad (2)$$

$$Z_{re} = R_{ct} + R_s + \sigma\omega^{-1/2} \quad (3)$$

where $R$ is the gas constant, $A$ the surface area of the cathode, $T$ the absolute temperature, $F$ the Faraday constant, $n$ the number of electrons transferred in the half-reaction for the redox couple, and $C_{Li}$ the concentration of lithium ion in solid. The Warburg factor, $\sigma$, is relative to $Z_{re} - \sigma$ and can be obtained from the slope of the lines in Figure 11. The calculated lithium

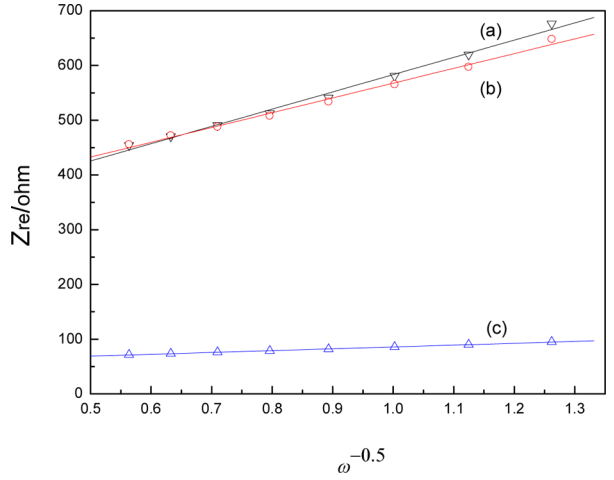


**Figure 11.** Graph of $Z_{re}$ plotted against $\omega^{-1/2}$ at a low-frequency region for the as-prepared samples with different molar ratio between Li and Ti: (a) Li/Ti = 4.5:5, (b) Li/Ti = 4:5, and (c) Li/Ti = 3.8:5.

ion diffusion coefficients are shown in Table 1. It can be seen that the lithium ion diffusion coefficients of $Li_4Ti_5O_{12}$−$TiO_2$ composites are higher than pristine $Li_4Ti_5O_{12}$. In addition, $Li_4Ti_5O_{12}$−$TiO_2$ composite (Li/Ti = 3.8:5) shows the highest diffusion coefficient among all samples, which is almost 100 times higher than that of pristine $Li_4Ti_5O_{12}$. To further investigate the effect of $TiO_2$ modification on the migration ability of lithium ion at a high charge−discharge rate, the lithium ion diffusion coefficients ($D_{Li}$) of $Li_4Ti_5O_{12}$ and $Li_4Ti_5O_{12}$−$TiO_2$ (Li/Ti = 3.8:5) samples charge−discharged at 10 C rate after 100 cycles at 100% charge state (charged to 2.5 V) are also calculated and given in the Supporting Information. The result is that $Li_4Ti_5O_{12}$−$TiO_2$ composite has a much higher lithium diffusion coefficient than pristine $Li_4Ti_5O_{12}$ due to the $TiO_2$ modification. This clearly indicates that the lithium-ion mobility at high charge−discharge rate can be effectively improved by $TiO_2$ modification. This is why the $Li_4Ti_5O_{12}$−$TiO_2$ nanocomposites show the higher rate capacity and cycling stability than pristine $Li_4Ti_5O_{12}$ during fast charge−discharge (Figure 8).

According to our synthesis process, the model of $Li_4Ti_5O_{12}$−$TiO_2$ nanocomposites can be shown in Figure 12. $Li^+$ ions from 8a site and Li counter electrode move to 16c sites of $Li_4Ti_5O_{12}$ during the discharge process. Hence, it can be concluded that the occupation of $Li^+$ ions at 16c site can impede $Li^+$ insertion and extraction,[66] resulting in the small Li diffusion coefficient

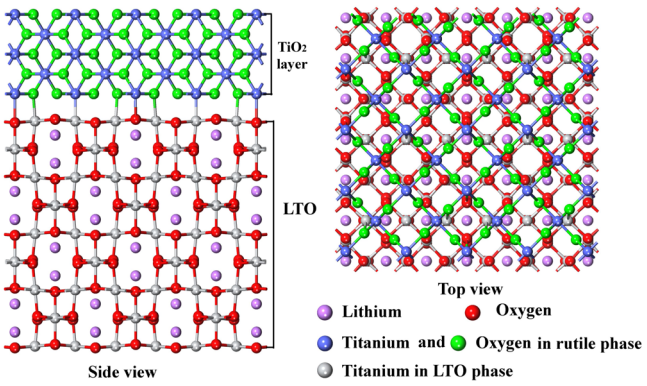


**Figure 12.** Model of $Li_4Ti_5O_{12}$–$TiO_2$ nanocomposites.

and poor rate capacity. However, the Li diffusion coefficient of rutile $TiO_2$ along the *c* axis ($10^{-6}$ $cm^2$ $s^{-1}$[67]) is much higher than $Li_4Ti_5O_{12}$.

It has been reported that lithium ions can react with the grain boundary phase in polycrystalline materials or the liquid electrolyte at the solid/liquid interface.[68] According to Figure12, in the $Li_4Ti_5O_{12}$–$TiO_2$ sample, in situ generated rutile–$TiO_2$ is tightly combined with $Li_4Ti_5O_{12}$ nanosheets or nanotubes, and then many rutile–$TiO_2$/$Li_4Ti_5O_{12}$ phase interfaces can be formed. The combined in situ generated rutile–$TiO_2$ can improve the Li diffusion coefficient along *c* axis. In addition, the interfaces can store electrolyte and provide more places for the insertion/extraction reactions of lithium ions, and then the reaction kinetics was improved,[60] leading to the observed low electrochemical polarization during the charge–discharge. It can be concluded that this is why the $Li_4Ti_5O_{12}$–$TiO_2$ nanocomposites show higher rate capacity and cycling stability than pristine $Li_4Ti_5O_{12}$ during fast charge–discharge (Figure 8). Hence, $TiO_2$ in situ modification is an effective way to improve the electrochemical performance of $Li_4Ti_5O_{12}$. The same strategy adopted in this work could be helpful to exploring and developing desired anode materials for advanced lithium-ion batteries.

## 4. CONCLUSIONS

Good-quality $Li_4Ti_5O_{12}$ and $Li_4Ti_5O_{12}$–$TiO_2$ nanocomposite anodes were successfully synthesized by the polyethylene glycol-assisted solvothermal method. All nanocomposites consisted of irregular nanosheets and nanotubes. The combination of in situ generated rutile–$TiO_2$ with $Li_4Ti_5O_{12}$ nanosheets or nanotubes is beneficial for improving the reversible intercalation and deintercalation of $Li^+$ and can provide more places for the insertion/extraction reactions of lithium ions, leading to the improvement of the reaction kinetics. $Li_4Ti_5O_{12}$–$TiO_2$ nanocomposites (Li/Ti = 3.8:5) anode exhibits the lowest charge-transfer resistance and the highest lithium diffusion coefficient among all samples, and it thus has a high reversibility and good rate capability. It should be highlighted that the as-prepared $Li_4Ti_5O_{12}$–$TiO_2$ nanocomposites (Li/Ti = 3.8:5) show a potential advantage in response to the increasing demands for high-power battery applications due to its outstanding rapid charge–discharge performance.

## ■ ASSOCIATED CONTENT

### Supporting Information

EIS of $Li_4Ti_5O_{12}$ and $Li_4Ti_5O_{12}$–$TiO_2$ nanocomposite charge–discharged at 10 C rate after 100 cycles. This material is available free of charge via the Internet at http://pubs.acs.org.

## ■ AUTHOR INFORMATION

### Corresponding Authors

*E-mail: tfyihit@163.com. Tel.: +86–555 2311807. Fax: +86 555 2311552.

*E-mail: xieying@hlju.edu.cn.

### Author Contributions

The manuscript was written with the contributions of all authors. All authors approved the final version of the manuscript.

### Notes

The authors declare no competing financial interest.

## ■ ACKNOWLEDGMENTS

This work was financially supported by the National Natural Science Foundation of China (nos. 51274002 and 51404002), the Anhui Provincial Natural Science Foundation, the Postdoctoral Science Research Development Foundation of Heilongjiang Province (no. LBH-Q13138), the Specialized Research Fund for the Doctoral Program of Higher Education (no. 20132301120001), and the Program for Innovative Research Team in Anhui University of Technology (no. TD201202).

## ■ REFERENCES

(1) Su, L.; Jing, Y.; Zhou, Z. Li Ion Battery Materials with Core–Shell Nanostructures. *Nanoscale* **2011**, *3*, 3967–3983.

(2) Li, H.; Wang, Z. X.; Chen, L. Q.; Huang, X. J. Research on Advanced Materials for Li-Ion Batteries. *Adv. Mater.* **2009**, *21*, 4593–4607.

(3) Chen, Z.; Belharouak, I.; Sun, Y.-K.; Amine, K. Titanium-based Anode Materials for Safe Lithium-Ion Batteries. *Adv. Funct. Mater.* **2013**, *23*, 959–969.

(4) Yang, J.; Zhou, X.-Y.; Zou, Y.-L.; Tang, J.-J. A Hierarchical Porous Carbon Material for High Power Lithium Ion Batteries. *Electrochim. Acta* **2011**, *56*, 8576–8581.

(5) Tan, L. P.; Lu, Z.; Tan, H. T.; Zhu, J.; Rui, X.; Yan, Q.; Huang, H. H. Germanium Nanowires-based Carbon Composite as Anodes for Lithium-Ion Batteries. *J. Power Sources* **2012**, *206*, 253–258.

(6) Goriparti, S.; Miele, E.; Angelis, F. D.; Fabrizio, E. D.; Zaccaria, R. P.; Capiglia, C. Review on Recent Progress of Nanostructured Anode Materials for Li-Ion Batteries. *J. Power Sources* **2014**, *257*, 421–443.

(7) Sun, Y.; Zhao, L.; Pan, H.; Lu, X.; Gu, L.; Hu, Y.-S.; Li, H.; Armand, M.; Ikuhara, Y.; Chen, L.; Huang, X. Direct Atomic-Scale Confirmation of Three-Phase Storage Mechanism in $Li_4Ti_5O_{12}$ Anodes for Room-Temperature Sodium-Ion Batteries. *Nat. Commun.* **2013**, *4*, 1870–1879.

(8) Zhang, B.; Yu, Y.; Liu, Y.; Huang, Z.-D.; He, Y.-B.; Kim, J.-K. Percolation Threshold of Graphene Nanosheets as Conductive Additives in $Li_4Ti_5O_{12}$ Anodes of Li-Ion Batteries. *Nanoscale* **2013**, *5*, 2100–2106.

(9) He, Y.-B.; Ning, F.; Li, B.; Song, Q.-S.; Lv, W.; Du, H.; Zhai, D.; Su, F.; Yang, Q.-H.; Kang, F. Carbon Coating to Suppress the Reduction Decomposition of Electrolyte on the $Li_4Ti_5O_{12}$ Electrode. *J. Power Sources* **2012**, *202*, 253–261.

(10) Wang, Y.-Q.; Gu, L.; Guo, Y.-G.; Li, H.; He, X.-Q.; Tsukimoto, S.; Ikuhara, Y.; Wan, L.-J. Rutile–$TiO_2$ Nanocoating for a High-Rate $Li_4Ti_5O_{12}$ Anode of a Lithium-Ion Battery. *J. Am. Chem. Soc.* **2012**, *134*, 7874–7879.

(11) Gao, Y.; Wang, Z.; Chen, L. Stability of Spinel $Li_4Ti_5O_{12}$ in Air. *J. Power Sources* **2014**, *245*, 684−690.
(12) Yi, T.-F.; Xie, Y.; Zhu, Y.-R.; Zhu, R.-S.; Shen, H. Structural and Thermodynamic Stability of $Li_4Ti_5O_{12}$ Anode Material for Lithium-Ion Battery. *J. Power Sources* **2013**, *222*, 448−454.
(13) Shen, L.; Yuan, C.; Luo, H.; Zhang, X.; Yang, S.; Lu, X. In Situ Synthesis of High-Loading $Li_4Ti_5O_{12}$−Graphene Hybrid Nanostructures for High Rate Lithium Ion Batteries. *Nanoscale* **2011**, *3*, 572−574.
(14) Wang, G. J.; Gao, J.; Fu, L. J.; Zhao, N. H.; Wu, Y. P.; Takamura, T. Preparation and Characteristic of Carbon-Coated $Li_4Ti_5O_{12}$ Anode Material. *J. Power Sources* **2007**, *174*, 1109−1112.
(15) Yi, T.-F.; Yang, S.-Y.; Li, X.-Y.; Yao, J.-H.; Zhu, Y.-R.; Zhu, R.-S. Sub-Micrometric $Li_{4-x}Na_xTi_5O_{12}$ ($0 \le x \le 0.2$) Spinel as Anode Material Exhibiting High Rate Capability. *J. Power Sources* **2014**, *246*, 505−511.
(16) Yi, T.-F.; Liu, H.; Zhu, Y.-R.; Jiang, L.-J.; Xie, Y.; Zhu, R.-S. Improving the High Rate Performance Of $Li_4Ti_5O_{12}$ through Divalent Zinc Substitution. *J. Power Sources* **2012**, *215*, 258−265.
(17) Zhang, Q.; Zhang, C.; Li, B.; Kang, S.; Li, X.; Wang, Y. Preparation and Electrochemical Properties of Ca-Doped $Li_4Ti_5O_{12}$ as Anode Materials in Lithium-Ion Battery. *Electrochim. Acta* **2013**, *98*, 146−152.
(18) Wang, W.; Jiang, B.; Xiong, W.; Wang, Z.; Jiao, S. A Nanoparticle Mg-Doped $Li_4Ti_5O_{12}$ for High Rate Lithium-Ion Batteries. *Electrochim. Acta* **2013**, *114*, 198−204.
(19) Capsoni, D.; Bini, M.; Massarotti, V.; Mustarelli, Pi.; Ferrari, S.; Chiodelli, G.; Mozzati, M. C.; Galinetto, P. Cr and Ni Doping of $Li_4Ti_5O_{12}$: Cation Distribution and Functional Properties. *J. Phys. Chem. C* **2009**, *113*, 19664−19671.
(20) Zhao, H.; Li, Y.; Zhu, Z.; Lin, J.; Tian, Z.; Wang, R. Structural and Electrochemical Characteristics of $Li_{4-x}Al_xTi_5O_{12}$ as Anode Material For Lithium-Ion Batteries. *Electrochim. Acta* **2008**, *53*, 7079−7083.
(21) Zhang, Y.; Zhang, C.; Lin, Y.; Xiong, D.-B.; Wang, D.; Wu, X.; He, D. Influence of $Sc^{3+}$ Doping in B-Site on Electrochemical Performance of $Li_4Ti_5O_{12}$ Anode Materials for Lithium-Ion Battery. *J. Power Sources* **2014**, *250*, 50−57.
(22) Yi, T.-F.; Xie, Y.; Wu, Q.; Liu, H.; Jiang, L.; Ye, M.; Zhu, R. High Rate Cycling Performance of Lanthanum-Modified $Li_4Ti_5O_{12}$ Anode Materials for Lithium-Ion Batteries. *J. Power Sources* **2012**, *214*, 220−226.
(23) Wang, W.; Wang, H.; Wang, S.; Hu, Y.; Tian, Q.; Jiao, S. Ru-doped $Li_4Ti_5O_{12}$ Anode Materials for High Rate Lithium-ion Batteries. *J. Power Sources* **2013**, *228*, 244−249.
(24) Li, X.; Tang, S.; Qu, M.; Huang, P.; Li, W.; Yu, Z. A Novel Spherically Porous Zr-doped Spinel Lithium Titanate ($Li_4Ti_{5-x}Zr_xO_{12}$) for High Rate Lithium Ion Batteries. *J. Alloys Compd.* **2014**, *588*, 17−24.
(25) Yang, C.-C.; Hu, H.-C.; Lin, S. J.; Chen, W.-C. Electrochemical Performance of V-Doped Spinel $Li_4Ti_5O_{12}$/C Composite Anode in Li-Half and $Li_4Ti_5O_{12}$/$LiFePO_4$-Full Cell. *J. Power Sources* **2014**, *258*, 424−433.
(26) Yi, T.-F.; Xie, Y.; Shu, J.; Wang, Z.; Yue, C.-B.; Zhu, R.-S.; Qiao, H.-B. Structure and Electrochemical Performance of Niobium-Substituted Spinel Lithium Titanium Oxide Synthesized by Solid-State Method. *J. Electrochem. Soc.* **2011**, *158*, A266−A274.
(27) Zhang, Q.; Zhang, C.; Li, B.; Jiang, D.; Kang, S.; Wang, X. Y. Preparation and Characterization of W-Doped $Li_4Ti_5O_{12}$ Anode Material for Enhancing the High Rate Performance. *Electrochim. Acta* **2013**, *107*, 139−146.
(28) Yi, T.-F.; Xie, Y.; Jiang, L.-J.; Shu, J.; Yue, C.-B.; Zhou, A.-N.; Ye, M.-F. Advanced Electrochemical Properties of Mo-Doped $Li_4Ti_5O_{12}$ Anode Material for Power Lithium Ion Battery. *RSC Adv.* **2012**, *2*, 3541−3547.
(29) Zhao, Z.; Xu, Y.; Ji, M.; Zhang, H. Synthesis and Electrochemical Performance of F-Doped $Li_4Ti_5O_{12}$ for Lithium-Ion Batteries. *Electrochim. Acta* **2013**, *109*, 645−650.
(30) Jung, H.-G.; Myung, S.-T.; Yoon, C. S.; Son, S.-B.; Oh, K. H.; Amine, K.; Scrosati, B.; Sun, Y.-K. Microscale Spherical Carbon-Coated $Li_4Ti_5O_{12}$ as Ultra High Power Anode Material for Lithium Batteries. *Energy Environ. Sci.* **2011**, *4*, 1345−1351.
(31) Jian, Z.; Zhao, L.; Wang, R.; Hu, Y.-S.; Li, H.; Chen, W.; Chen, L. The Low-Temperature (400 °C) Coating of Few-Layer Graphene on Porous $Li_4Ti_5O_{12}$ via $C_{28}H_{16}Br_2$ Pyrolysis for Lithium-Ion Batteries. *RSC Adv.* **2012**, *2*, 1751−1754.
(32) Li, N.; Liang, J.; Wei, D.; Zhu, Y.; Qian, Y. Solvothermal Synthesis of Micro-/Nanoscale Cu/$Li_4Ti_5O_{12}$ Composites for High Rate Li-Ion Batteries. *Electrochim. Acta* **2014**, *123*, 346−352.
(33) Krajewski, M.; Michalska, M.; Hamankiewicz, B.; Ziolkowska, D.; Korona, K. P.; Jasinski, J. B.; Kaminska, M.; Lipinska, L.; Czerwinski, A. $Li_4Ti_5O_{12}$ Modified with Ag Nanoparticles as an Advanced Anode Material in Lithium-Ion Batteries. *J. Power Sources* **2014**, *245*, 764−771.
(34) Li, C. C.; Li, Q. H.; Chen, L. B.; Wang, T. H. A Facile Titanium Glycolate Precursor Route to Mesoporous Au/$Li_4Ti_5O_{12}$ Spheres for High-Rate Lithium-Ion Batteries. *ACS Appl. Mater. Interfaces* **2012**, *4*, 1233−1238.
(35) Liu, G.-Y.; Wang, H.-Y.; Liu, G.-Q.; Yang, Z.-Z.; Jin, B.; Jiang, Q.-C. Synthesis and Electrochemical Performance of High-Rate Dual-Phase $Li_4Ti_5O_{12}$−$TiO_2$ Nanocrystallines for Li-Ion Batteries. *Electrochim. Acta* **2013**, *87*, 218−223.
(36) Tang, Y.; Tan, X.; Hou, G.; Zheng, G. Nanocrystalline $Li_4Ti_5O_{12}$-Coated $TiO_2$ Nanotube Arrays as Three-Dimensional Anode for Lithium-Ion Batteries. *Electrochim. Acta* **2014**, *117*, 172−178.
(37) Liu, J.; Li, X.; Cai, M.; Li, R.; Sun, X. Ultrathin Atomic Layer Deposited $ZrO_2$ Coating to Enhance the Electrochemical Performance of $Li_4Ti_5O_{12}$ as an Anode Material. *Electrochim. Acta* **2013**, *93*, 195−201.
(38) Park, K.-S.; Benayad, A.; Kang, D.-J.; Doo, S.-G. Nitridation-Driven Conductive $Li_4Ti_5O_{12}$ for Lithium Ion Batteries. *J. Am. Chem. Soc.* **2008**, *130*, 14930−14931.
(39) Li, W.; Li, X.; Chen, M.; Xie, Z.; Zhang, J.; Dong, S.; Qu, M. $AlF_3$ Modification to Suppress the Gas Generation of $Li_4Ti_5O_{12}$ Anode Battery. *Electrochim. Acta* **2014**, *139*, 104−110.
(40) Yi, T.-F.; Yang, S.-Y.; Tao, M.; Xie, Y.; Zhu, Y.-R.; Zhu, R.-S. Synthesis and Application of a Novel $Li_4Ti_5O_{12}$ Composite as Anode Material with Enhanced Fast Charge−Discharge Performance for Lithium-Ion Battery. *Electrochim. Acta* **2014**, *134*, 377−383.
(41) Wang, X.; Shen, L.; Li, H.; Wang, J.; Dou, H.; Zhang, X. PEDOT Coated $Li_4Ti_5O_{12}$ Nanorods: Soft Chemistry Approach Synthesis and Their Lithium Storage Properties. *Electrochim. Acta* **2014**, *129*, 283−289.
(42) Ganapathy, S.; Wagemaker, M. Nanosize Storage Properties in Spinel $Li_4Ti_5O_{12}$ Explained By Anisotropic Surface Lithium Insertion. *ACS Nano* **2012**, *6*, 8702−8712.
(43) Cheng, L.; Yan, J.; Zhu, G.-N.; Luo, J.-Y.; Wang, C.-X.; Xia, Y.-Y. General Synthesis of Carbon-Coated Nanostructure $Li_4Ti_5O_{12}$ as a High Rate Electrode Material for Li-Ion Intercalation. *J. Mater. Chem.* **2010**, *20*, 595−602.
(44) Jeong, G.; Kim, Y.-U.; Kim, H.; Kim, Y.-J.; Sohn, H.-J. Prospective Materials and Applications for Li Secondary Batteries. *Energy Environ. Sci.* **2011**, *4*, 1986−2002.
(45) Pfanzelt, M.; Kubiak, P.; Fleischhammer, M.; Wohlfahrt-Mehrens, M. $TiO_2$ Rutile—An Alternative Anode Material for Safe Lithium-Ion Batteries. *J. Power Sources* **2011**, *196*, 6815−6821.
(46) Koudriachova, M. V.; Harrison, N. M.; Leeuw, S. W. Effect of Diffusion on Lithium Intercalation in Titanium Dioxide. *Phys. Rev. Lett.* **2001**, *86*, 1275.
(47) Zhang, C.; Zhang, Y.; Wang, J.; Wang, D.; He, D.; Xia, Y. $Li_4Ti_5O_{12}$ Prepared by A Modified Citric Acid Sol−Gel Method for Lithium-Ion Battery. *J. Power Sources* **2013**, *236*, 118−125.
(48) Li, X.; Lin, H.-c.; Cui, W.-j.; Xiao, Q.; Zhao, J.-b. Fast Solution-Combustion Synthesis of Nitrogen-Modified $Li_4Ti_5O_{12}$ Nanomaterials with Improved Electrochemical Performance. *ACS Appl. Mater. Interfaces* **2014**, *6*, 7895−7901.

(49) Bai, Y.; Wang, F.; Wu, F.; Wu, C.; Bao, L.-y. Influence of Composite LiCl–KCl Molten Salt on Microstructure and Electrochemical Performance of Spinel $Li_4Ti_5O_{12}$. *Electrochim. Acta* **2008**, *54*, 322–327.
(50) Yin, S. Y.; Song, L.; Wang, X. Y.; Zhang, M. F.; Zhang, K. L.; Zhang, Y. X. Synthesis of Spinel $Li_4Ti_5O_{12}$ Anode Material by A Modified Rheological Phase Reaction. *Electrochim. Acta* **2009**, *54*, 5629–5633.
(51) Zhang, W.; Li, J.; Guan, Y.; Jin, Y.; Zhu, W.; Guo, X.; Qiu, X. Nano-$Li_4Ti_5O_{12}$ with High Rate Performance Synthesized by a Glycerol Assisted Hydrothermal Method. *J. Power Sources* **2013**, *243*, 661–667.
(52) Wang, Y.; Cao, G. Developments in Nanostructured Cathode Materials for High-Performance Lithium-Ion Batteries. *Adv. Mater.* **2008**, *20*, 2251–2269.
(53) Bruce, P. G.; Scrosati, B.; Tarascon, J.-M. Nanomaterials for Rechargeable Lithium Batteries. *Angew. Chem., Int. Ed.* **2008**, *47*, 2930–2946.
(54) Devaraju, M. K.; Honma, I. Hydrothermal and Solvothermal Process Towards Development of $LiMPO_4$ (M = Fe, Mn) Nanomaterials for Lithium-Ion Batteries. *Adv. Energy Mater.* **2012**, *2*, 284–297.
(55) Tang, Y. F.; Yang, L.; Qiu, Z.; Huang, J. S. Template-Free Synthesis of Mesoporous Spinel Lithium Titanate Microspheres and Their Application in High-Rate Lithium Ion Batteries. *J. Mater. Chem.* **2009**, *19*, 5980–5984.
(56) Kubiak, P.; Pfanzelt, M.; Geserick, J.; Hümann, U.; Hüsing, N.; Kaiser, U.; Wohlfahrt-Mehrens, M. Electrochemical Evaluation of Rutile $TiO_2$ Nanoparticles as Negative Electrode for Li-Ion Batteries. *J. Power Sources* **2009**, *194*, 1099–1104.
(57) Marinaro, M.; Pfanzelt, M.; Kubiak, P.; Marassi, R.; Wohlfahrt-Mehrens, M. Low Temperature Behaviour of $TiO_2$ Rutile as Negative Electrode Material for Lithium-Ion Batteries. *J. Power Sources* **2011**, *196*, 9825–9829.
(58) Wang, J.; Zhao, H.; Yang, Q.; Wang, C.; Lv, P.; Xia, Q. $Li_4Ti_5O_{12}$–$TiO_2$ Composite Anode Material for Lithium-Ion Batteries. *J. Power Sources* **2013**, *222*, 196–201.
(59) Wang, D.; Choi, D.; Li, J.; Yang, Z.; Nie, Z.; Kou, R.; Hu, D.; Wang, C.; Saraf, L. V.; Zhang, J.; Aksay, I. A.; Liu, J. Self-Assembled $TiO_2$–Graphene Hybrid Nanostructures for Enhanced Li-Ion Insertion. *ACS Nano* **2009**, *3*, 907.
(60) Rahman, M. M.; Wang, J.-Z.; Hassan, M. F.; Wexler, D.; Liu, H. K. Amorphous Carbon Coated High Grain Boundary Density Dual Phase $Li_4Ti_5O_{12}$-$TiO_2$: A Nanocomposite Anode Material for Li-Ion Batteries. *Adv. Energy Mater.* **2011**, *1*, 212–220.
(61) Liao, J.-Y.; Xiao, X.; Higgins, D.; Lee, D.; Hassan, F.; Chen, Z. Hierarchical $Li_4Ti_5O_{12}$–$TiO_2$ Composite Microsphere Consisting of Nanocrystals for High Power Li-Ion Batteries. *Electrochim. Acta* **2013**, *108*, 104–111.
(62) Wang, B.; Wang, J.; Cao, J.; Ge, H.; Tang, Y. Nitrogen-Doped $Li_4Ti_5O_{12}$ Nanosheets with Enhanced Lithium Storage Properties. *J. Power Sources* **2014**, *266*, 150–154.
(63) Chou, S.-L.; Wang, J.-Z.; Liu, H.-K.; Dou, S.-X. Rapid Synthesis of $Li_4Ti_5O_{12}$ Microspheres as Anode Materials and Its Binder Effect for Lithium-Ion Battery. *J. Phys. Chem. C* **2011**, *115*, 16220–16227.
(64) Zhou, X.-Y.; Tang, J.-J.; Yang, J.; Zou, Y.-L.; Wang, S.-C.; Xie, J.; Ma, L.-L. Effect of Polypyrrole on Improving Electrochemical Performance of Silicon Based Anode Materials. *Electrochim. Acta* **2012**, *70*, 296–303.
(65) Zhou, X.; Tang, J.; Yang, J.; Xie, J.; Huang, B. Seaweed-Like Porous Carbon from the Decomposition of Polypyrrole Nanowires for Application in Lithium Ion Batteries. *J. Mater. Chem. A* **2013**, *1*, 5037–5044.
(66) Lin, C.; Fan, X.; Xin, Y.; Cheng, F.; Lai, M. O.; Zhou, H.; Lu, L. Monodispersed Mesoporous $Li_4Ti_5O_{12}$ Submicrospheres as Anode Materials for Lithium-Ion Batteries: Morphology and Electrochemical Performances. *Nanoscale* **2014**, *6*, 6651–6660.
(67) Dong, S.; Wang, H.; Gu, L.; Zhou, X.; Liu, Z.; Han, P.; Wang, Y.; Chen, X.; Cui, G.; Chen, L. Rutile $TiO_2$ Nanorod Arrays Directly Grown on Ti Foil Substrates Towards Lithium-Ion Micro-Batteries. *Thin Solid Films* **2011**, *519*, 5978–5982.
(68) Beaulieu, L. Y.; Larcher, D.; Dunlap, R. A.; Dahn, J. R. Reaction of Li with Grainboundary Atoms in Nanostructured Compounds. *J. Electrochem. Soc.* **2000**, *147*, 3206–3212.